

Biomimetic folding of triangular deployable membranes

Yuzhen Tang^{1,*}, P. Beccarelli², Hongwei Guo¹, Rongqiang Liu¹, D.S.A. De Focatiis² and Zongquan Deng¹

¹ State Key Laboratory of Robotics and System, Harbin Institute of Technology, Harbin 150001, China

² Faculty of Engineering, University of Nottingham, Nottingham NG7 2RD, United Kingdom

*Corresponding authors, tangyuzhen@hit.edu.cn

Abstract:

Recently membrane deployable mechanisms have been increasingly applied for numerous space projects owing to their capacity for large scales, light weight and small stowage volumes. The geometric design of biomimetic folding is studied to design creases patterns of triangular deployable membranes applied in space. Various crease designs for triangular membrane based on leaf-in, leaf-out and orthogonal pattern are put forward, especially the patterns composed of triangular and hexagonal units. In order to analyse the membrane folding method based on biomimetic folding, a set of evaluation indices, including linear dimension ratio, deployment ratio, creases length and junction number, are established. The indices of various membrane folding patterns are calculated according to the crease distributions and geometric relations. Furthermore, a parametric study of crease parameters is performed to determine how the parameters affect the folding behaviours and deployment efficiencies. These indices can provide an indication to aid with the selection of crease patterns and folding parameters for triangular deployable membranes according to the required performance and space mission requirements.

Keywords: biomimetic folding, deployable membrane, geometric design, evaluation indices

1 Introduction

With an increasing demand for large-scale space structures such as solar panels, antennas and solar sails, deployable mechanisms have been attracting significant recent interest. In comparison with traditional rigid deployable mechanisms, membrane deployable mechanisms can be substantially larger in scale, while still being

lightweight, package to smaller stowage volumes, and be produced at lower costs (Zhiquan Liu 2017). Origami, the traditional art of paper folding (Peraza Hernandez 2018), has inspired the design and functionality of deployable and foldable structures (Y. Chen 2015) for decades. In particular, space engineering applications of origami have started to gather attention in recent years, especially in the field of folding method design for membranes (Nicholas Turner 2016).

Space deployable membrane technology is particularly applicable to space membrane antennas, membrane solar cell arrays, large area solar sails and space solar power stations. Both NASA (Chodimella, Moore et al. 2006) and the European Space Agency (ESA) (Leipold, Widani et al. 2006) have developed prototypes of planar and curved membrane antennas, and NASA has already carried out in-orbit tests. The membrane antenna requires both a reliable deployment and a high level of surface accuracy. Solar cell arrays have been developed as either rigid structures or as flexible membrane structures (Talley, Clayton et al. 2006, Trautt and White 2013, Bao, White et al. 2016), and membrane structures have advantages in areal density and power to mass ratio. Examples include the IKAROS (Interplanetary Kite-craft Accelerated by Radiation Of the Sun) solar sail (Mori Osamu 2010, Zicai Shen 2012) and the NanoSail-D solar sail (Alhorn Dean, Agasid et al. 2011, Les Johnson 2011), both of which are membrane sails based on origami. In typical space solar power station schemes, such as the 'Sun Tower' Solar Power Satellite (Mankins 2002), the Tethered-SPS (Sasaki, Tanaka et al. 2007), the SPS-ALPHA (Mankins, Kaya et al. 2012) and the SSPS-OMEGA (Yang, Zhang et al. 2016), kilometre-size membrane condensers are necessary. In order to address the conflict between the large scales required of the deployed space membranes and the dimensional constraints of the launch capability, origami can provide solutions based on folding arrangements during launch that are unfolded in orbit. Origami approaches that have been proposed include the Miura-ori (Koryo 1985), the inextensional wrapping (Guest 1992) and the rotationally skew fold approach (Furuya, Inoue et al. 2005). One of the challenges of space applications of origami is to accommodate finite thickness in origami-based deployable solar arrays with a high deployment ratio (Zirbel, Lang et al. 2013, Zirbel, Trease et al. 2015).

Biomimetic folding, inspired by the manner in which structures in nature fold **being the result of millions of years of adaptation to life and ever-changing surroundings**, has provided inspiration towards new folding patterns (Kobayashi, Daimaruya et al. 2000). **Biomimetic leaf-folding with veins and midribs in leaves as stiffening members is the most popular imitation for the deployable membrane structures because of outstanding capabilities and balance of flexibility and rigidity.** A relatively simple and regular corrugated folding pattern was observed in leaves of hornbeam and beech (Kobayashi, Kresling et al. 1998), and another based on the unfolding mechanism of morning glory flowers (Kobayashi, Daimaruya et al. 2003). The foldable leaf pattern of the famous leaf folding

shrub, *Mimosa pudica*, has also been studied with the help of experiments and model simulations (H.S.Patil and SiddharthVaijapurkar 2007). A fundamental advantage of the leaf folding pattern is that, under certain circumstances, it is capable of unfolding with a single degree of freedom, which makes it appealing from the point of view of ease of deployment. The simple model of deploying tree leaves was later been assembled in different arrangements to produce polygonal foldable membranes that could be more readily applied to deployable space structures (Focatiis and Guest 2002). These leaf-like units were also utilized to design deployable pyramidal shelter structures (Jianguo Cai 2015), and contact issues during unfolding of leaf-based membranes were recently investigated by Yuan and coworkers (Yuan 2020).

One of the challenges of employing these biomimetic folding patterns in space applications is that the deployed geometry is generally made up of a large continuous surface, which is tessellated using smaller repeat units. Compared with the more common shapes squares and hexagons used for this purpose, triangles are capable of being assembled to the latter and divided into various combinations to obtain novel creases patterns because of its unique symmetry. Thus the folding triangular unit forms an important basis for the development of large foldable surfaces. Moreover, another challenge is to refine evaluation indices from space mission requirements and apply to triangular deployable membranes based on biomimetic folding, which has been considered in few researches so far. Most well-known evaluation indices in deployable membrane research have focused on areal density, total weight, strain energy and shape accuracy RMS (Root Mean Square), which are still limited to assess the performance of deployable membrane directly, but incapable of being linked with folding patterns. These limitations have hindered the adoption of evaluation indices in practical applications, especially for assessment of biomimetic folding pattern in triangular deployable membranes and guidance on creases design. In this work the aim is to explore the different possible arrangements of biomimetic leaf-folding patterns to produce deployable triangles, and to compare and contrast measures of quality to aid designers in making the most appropriate selection of biomimetic folding patterns for specific space applications based on considerations of folding efficiency and complexity.

2 Geometric design of biomimetic folding

2.1 Basic unit of biomimetic folding

Fig. 1 describes the corrugated leaf model of hornbeam leaves based on the combination of multiple Miura-ori units. The solid lines indicate crest creases and the dashed lines indicate valley creases. Point O of the corrugated leaf model is the center point around which the n_l leaves in the pattern are arranged. The angle between the midrib

OX and the side veins, known as the vein angle α , can be used to distinguish between the leaf-in pattern and the leaf-out pattern. The leaves can be arranged in two basic ways, either (1) pointing towards the center, $\alpha > \frac{\pi}{2}$, leaf-in; or (2) directed away from it, $\alpha < \frac{\pi}{2}$, leaf-out. The basic unit is designed according to the corrugated leaf model, in which the angle between the boundary lines of the basic unit OA and OB shown is defined as 2β , which satisfies

$$2\beta = \frac{2\pi}{n_l} \quad (1)$$

In the leaf-in pattern, when the side veins are perpendicular to boundary lines of the basic unit OA and OB, the relation between α and β is

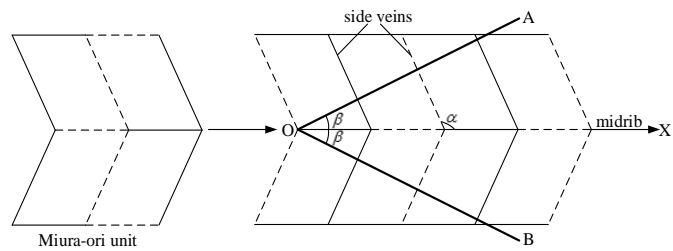
$$\alpha - \beta = \frac{\pi}{2} \quad (2)$$

Substituting the angle $\beta = \frac{\pi}{n_l}$ in Eq.(2), the angle α is then

$$\alpha = \frac{\pi}{2} + \frac{\pi}{n_l} \quad (3)$$



(a) Hornbeam leaves



(b) Basic unit based on the corrugated leaf model

Fig. 1: Basic unit based on the corrugated leaf model

Starting from the basic unit of the corrugated leaf model, the leaf-in patterns can be extended to regular polygons by arranging n_l basic units around Point O and bounding with the edges of the polygons, as illustrated in Fig. 2 (a, b, and c), adapting the values of α , β and the number of leaves n_l . The folded configurations of a triangular, square and hexagonal geometry are illustrated in paper models shown in Fig. 2 (d, e and f).

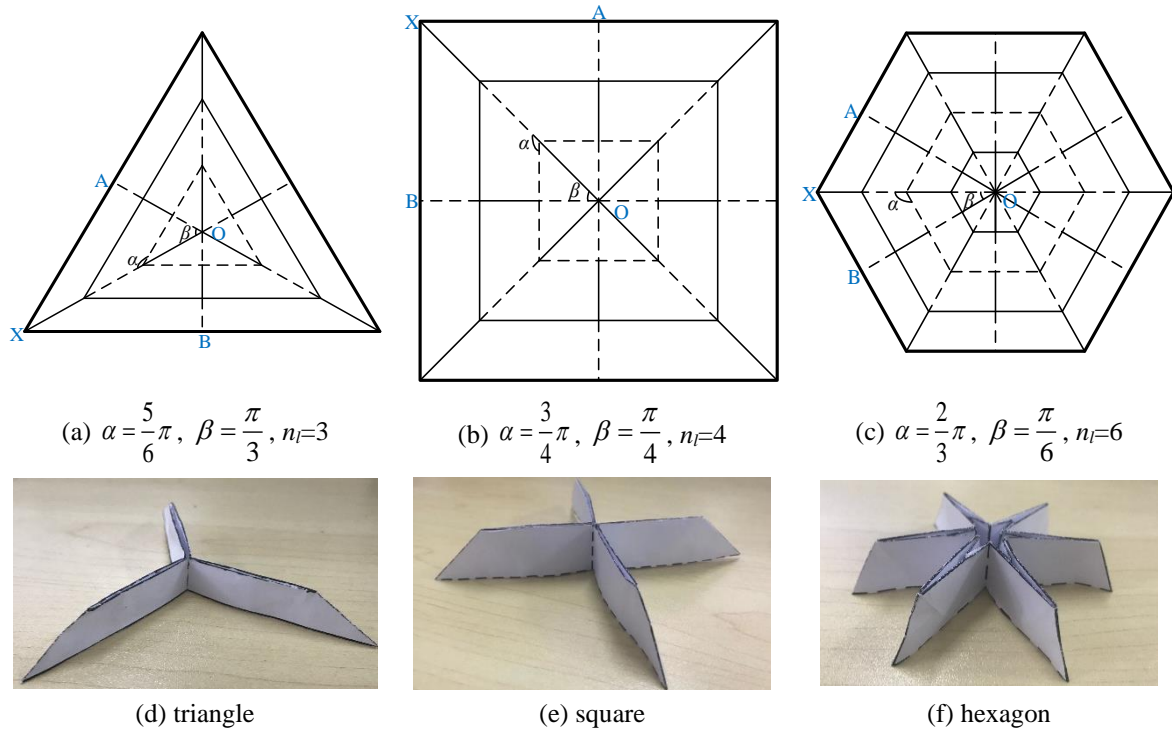


Fig. 2: Creases and folded configurations of traditional leaf-in pattern

The side veins of a leaf-out pattern are parallel to boundary lines of the basic unit OA and OB and the relation between α and β is $\alpha = \beta$. Fig. 3 describes the creases and folded configurations of the same triangular, square and hexagonal geometries based on the traditional leaf-out pattern.

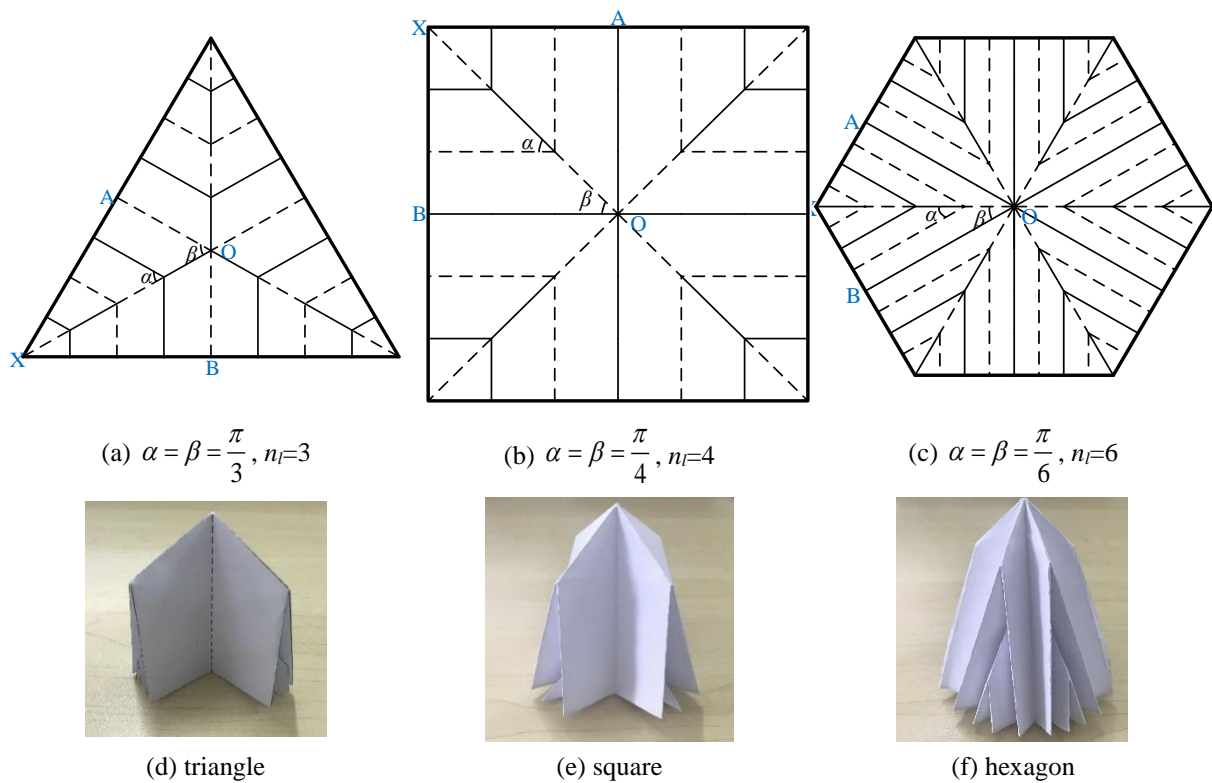


Fig. 3: Creases and folded configurations of traditional leaf-out pattern

As an alternative to the leaf-in and leaf-out patterns, Fig. 4 describes a corrugated leaf model based on a unit with

$\alpha = \frac{\pi}{2}$, here defined as orthogonal pattern, which can be used as starting point to develop further folding creases

patterns, as described in detail in section 2.2.1.

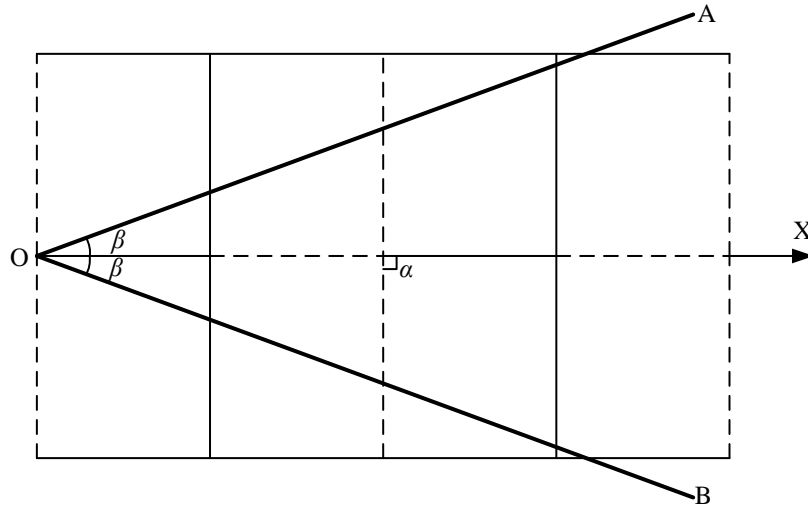


Fig. 4: Basic unit with $\alpha = \frac{\pi}{2}$ based on the corrugated leaf model

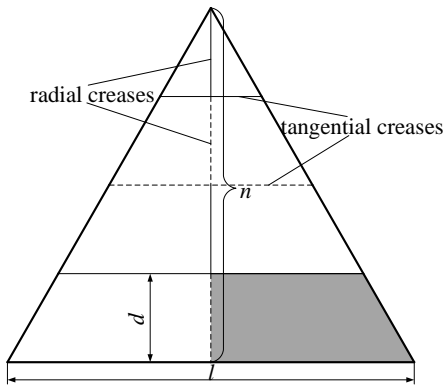
2.2 Triangular membrane based on basic unit of biomimetic folding

Triangular membranes have been extensively used in industry in the recent years because of their advantages in terms of modular design. In this section, the crease patterns of triangular membranes based on basic units of biomimetic folding are designed. Additionally, the folded configurations of various creases patterns are investigated by using paper models.

2.2.1 Triangle based on orthogonal pattern.

According to the basic unit with $\alpha = \frac{\pi}{2}$ based on the corrugated leaf model, creases of the triangle obtained from an orthogonal pattern can be designed and classified as tangential and radial creases, as shown in Fig. 5 (a). Its folded configuration is illustrated by the paper model in Fig. 5 (b), and consists of a prism of the same dimensions as the shaded parallelogram in Fig. 5 (a). In the creases diagram, l is the side length of the triangle unit, d is the length of a radial crease, and n represents the number of radial creases, so their relationship is obtained as

$$nd = \frac{\sqrt{3}}{2} l \quad (4)$$



(a) Creases diagram

(b) Folded configuration

Fig. 5: Creases diagram and folded configuration of the triangle based on orthogonal pattern

2.2.2 Three-way orthogonal pattern.

As illustrated in Fig. 6, three triangle units with $\alpha = \frac{\pi}{2}$ and one additional triangle placed at the centre can form a new and larger triangle. To achieve a new folding pattern, the creases of the central triangle need to be designed. Due to the symmetry of the whole geometry, the central triangle can be divided into three identical parts, and some creases need to be designed and added, shown in green in Fig. 6. Based on this, the crest creases and valley creases also need to be allocated, shown in blue in Fig. 6. Thus the creases and folded configuration of the new triangle membrane, defined as a three-way orthogonal pattern, are composed of three triangle units based on the orthogonal pattern. This arrangement has a small folded volume and good ease of deployment. As shown in the creases diagram, the side length of the triangle equals to $2l$ according to the definition of variables l , n and d mentioned above.

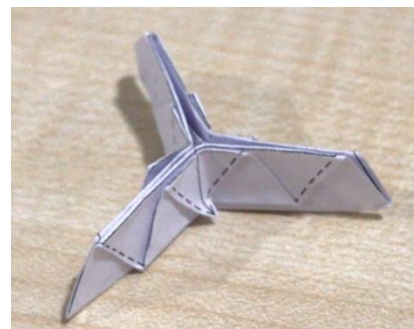
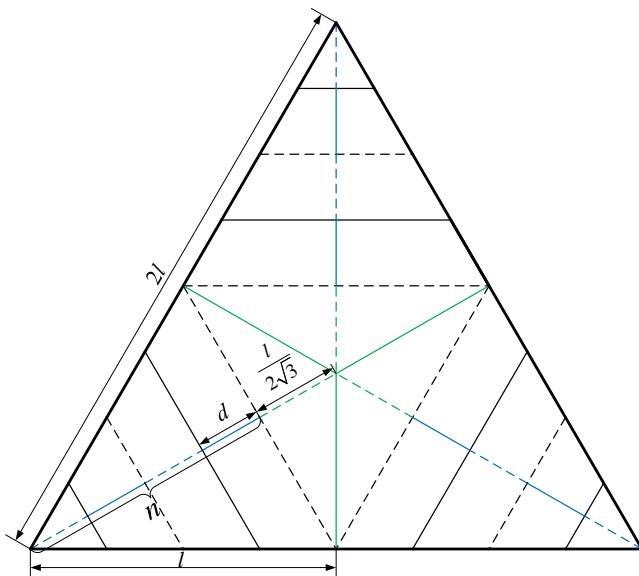
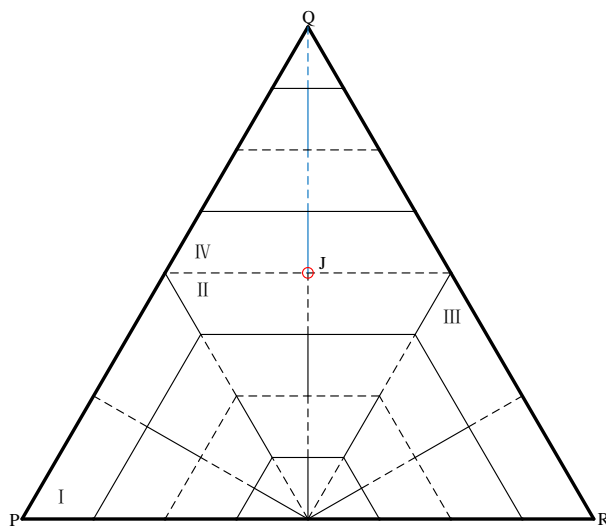


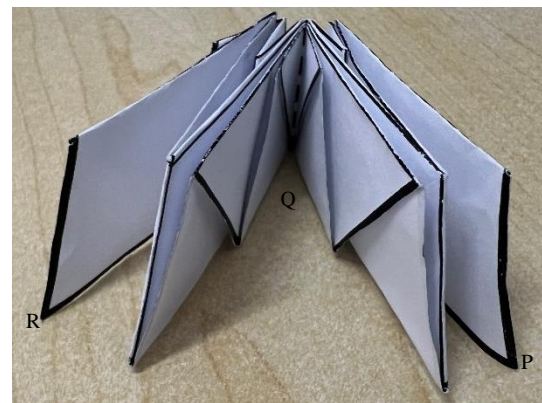
Fig. 6: Creases diagram and folded configuration of three-way orthogonal pattern

2.2.3 Four-way orthogonal pattern.

As shown in Fig. 7 (a), a new triangle made up of four triangle units with $\alpha = \frac{\pi}{2}$ is defined as a four-way orthogonal pattern; the individual triangles are labelled I, II, III and IV, respectively. However, four valley creases would intersect at the intersection of the central crease of triangle II and IV, labelled as point J and shown as a red circle. This would not be possible to fold. Hence, the crest radial creases and valley radial creases in triangle IV need to be inverted, and are redesigned and labelled as blue fold lines in Fig. 7 (a). Its folded configuration is illustrated in Fig. 7 (b). This pattern is deployed by tensioning three corners P, Q and R denoted in Fig. 7 (a), the apices of the large triangle, but when fully folded the corner Q is located inside and the other two corners P and R need to be tensioned first. In other words, these three corners cannot be tensioned simultaneously, and the four-way orthogonal pattern needs to be deployed in two separate sequence, which decreases the deployment efficiency. The first sequence is to tension corner P and R to expose corner Q, and then these three corners are applied tension simultaneously to achieve its deployed configuration of the flat triangular surface in the second sequence.



(a) Creases diagram



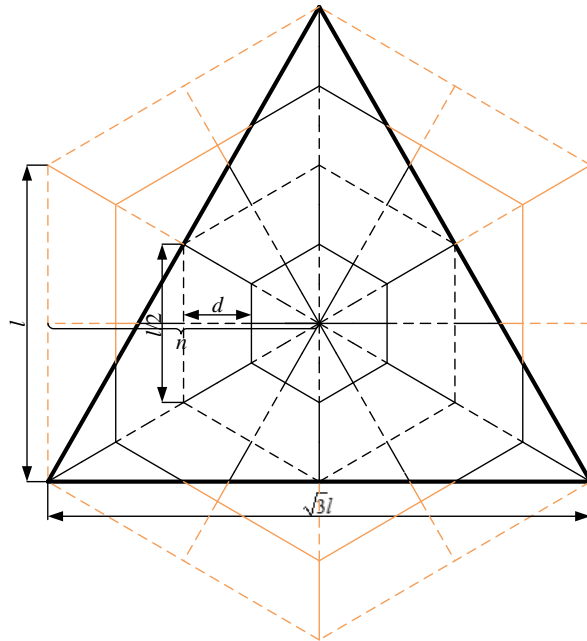
(b) Folded configuration

Fig. 7: Creases diagram and folded configuration of four-way orthogonal pattern

2.2.4 Triangle from hexagon based on leaf-in pattern.

As shown in Fig. 8 (a), creases design of a triangle can also be achieved from the creases of the hexagon based on leaf-in pattern plotted in green. Similarly, the definition of variables l , n and d are indicated in Fig. 8 (a), resulting

in the side length of the new triangle equals to $\sqrt{3}l$. Moreover, the folded configuration of the new triangle from hexagon based on leaf-in pattern is shown in Fig. 8 (b).



(a) Creases diagram



(b) Folded configuration

Fig. 8: Creases diagram and folded configuration of triangle from hexagon based on leaf-in pattern

2.2.5 Triangle based on leaf-out pattern.

The leaf-out pattern can also provide a starting point for a pattern of creases in the shape of a triangle. Its creases diagram and folded configuration are given in Fig. 3 (a) and (d). As illustrated in Fig. 9, this pattern is made up of six repeats of half of the triangle unit with $\alpha = \frac{\pi}{2}$, one of which is plotted in green. The relationship between the variables is kept consistent across patterns, and the definition of variables l , n and d are as indicated in Fig. 9.

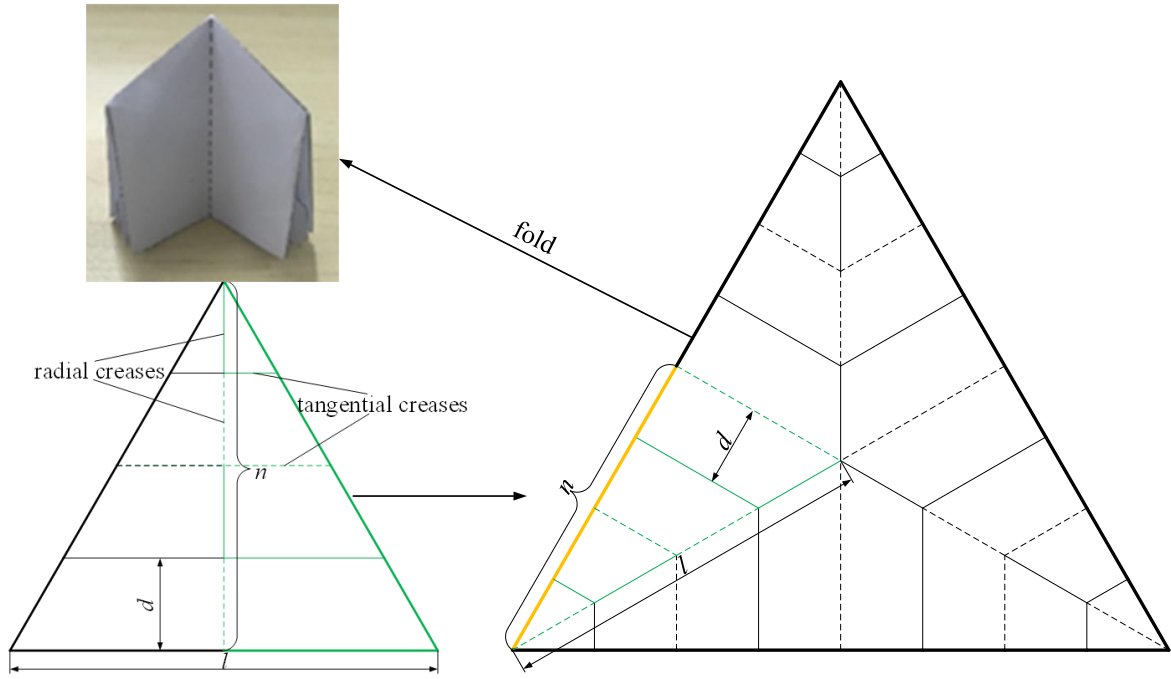


Fig. 9: Creases diagram and folded configuration of triangle based on leaf-out pattern

3 Evaluation Indices for Biomimetic Folding

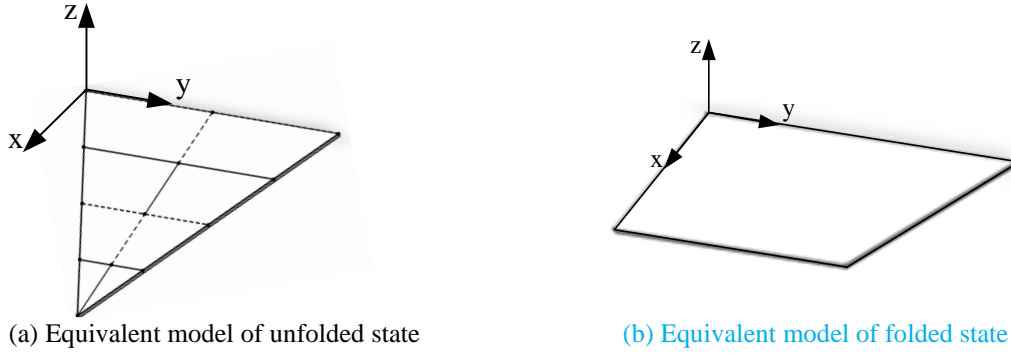
In order to satisfy the strict design requirements of foldable membrane structures for space applications (i.e. lightweight, high deployment ratio and large size) and to identify the best biomimetic folding pattern, we propose a series of evaluation indices designed to assess the folding patterns based on the origami concept. The following section explains how each evaluation index can be applied to the most promising patterns: the triangle based on an orthogonal pattern, the three-way orthogonal pattern, the triangle obtained from a hexagon based on leaf-in pattern and the triangle based on the leaf-out pattern.

3.1 Maximum linear dimension of folded configuration

The three-dimensional length of the launch vehicle imposes restrictions on the folded configuration of the space deployable membrane. As a result, the maximum linear dimension of the folded configuration is a key parameter to be considered. The approach here adopted to calculate the maximum linear dimension is based on an equivalent model given by the smallest polyhedron designed around the membrane in the unfolded and folded state. The effect of folding in a specific direction is described by the linear dimension ratio r_i , defined as the ratio between the maximum linear dimension of the unfolded configuration i_{\max}^u to the maximum linear dimension of the folded configuration i_{\max}^f , expressed as $r_i = i_{\max}^u / i_{\max}^f$ ($i=x, y, z$).

3.1.1 Triangle based on orthogonal pattern.

Based on the concept described in Fig. 5, the equivalent models of the unfolded and folded configuration of the triangle based on orthogonal pattern are illustrated in Fig. 10 (a) and (b) respectively.



(a) Equivalent model of unfolded state

(b) Equivalent model of folded state

Fig. 10: Equivalent model of unfolded and folded state of triangle based on orthogonal pattern

The maximum linear dimensions in the directions x , y and z are illustrated in Table 1, where s represents the membrane thickness. Combined with Eq.(4), it is possible to conclude that the linear dimension ratio r_i ($i=x, y, z$) is only dependent on the number of radial creases in a triangle unit n .

Table 1: Maximum linear dimension of the triangle based on orthogonal pattern

Direction ($i=x, y, z$)	x	y	z
i_{\max}^u	$\frac{\sqrt{3}}{2}l$	l	s
i_{\max}^f	$d\left(\frac{\sqrt{3}}{2n}l\right)$	$\frac{1}{2}l$	$2ns$
r_i	n	2	$\frac{1}{2n}$

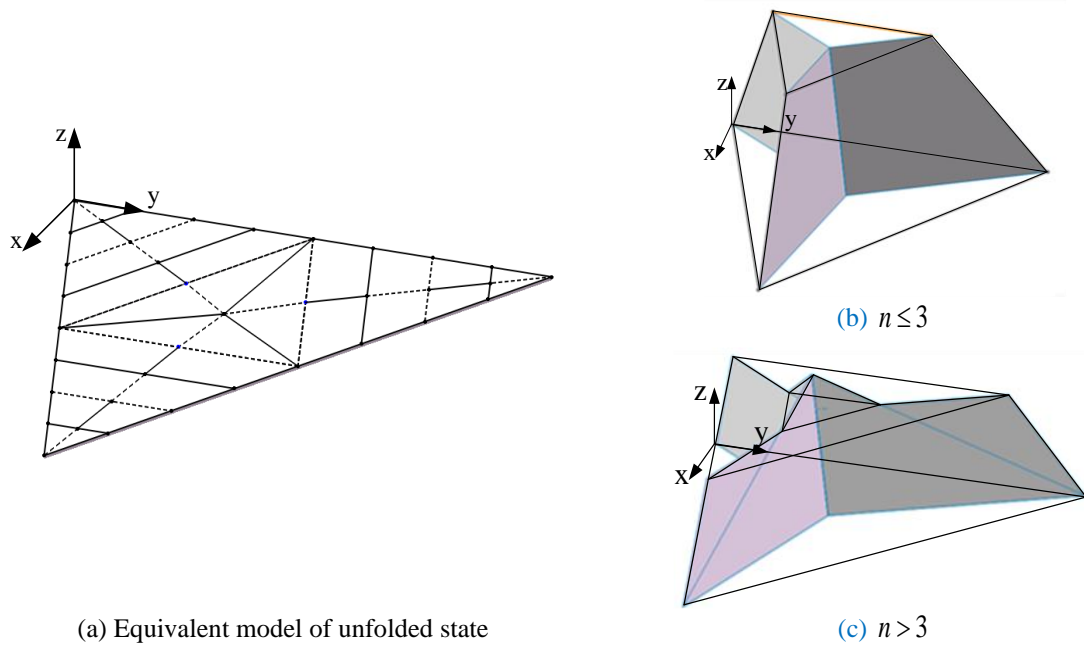
3.1.2 Three-way orthogonal pattern.

As shown in Fig. 11, the folded configuration of the three-way orthogonal pattern can be determined by the relationship between the length of a radial crease d and the length of $\frac{l}{2\sqrt{3}}$ in the central triangle shown in Fig. 6.

Eq.(5) shows that when $n=3$, d equals to the length of $\frac{l}{2\sqrt{3}}$, which means the case of $n=3$ is the critical state for the folded configuration.

Based on the geometric and numerical relationship, the equivalent models of the folded configurations of the three-way orthogonal pattern are shown in Fig. 11 (b) and (c) respectively, and the directions x , y , and z can be defined as shown in the figure. The maximum linear dimensions of the unfolded and folded configurations, and the linear dimension ratio in different directions are illustrated in Table 2.

$$d = \frac{\sqrt{3}}{2n}l = \frac{1}{2\sqrt{3}}l \quad (5)$$



(a) Equivalent model of unfolded state
Fig. 11: Equivalent models of the unfolded and folded states of the three-way orthogonal pattern: (a) Equivalent model in the unfolded state; (b) Equivalent model of the folded configuration when $n \leq 3$; (c) Equivalent model of the folded configuration when $n > 3$

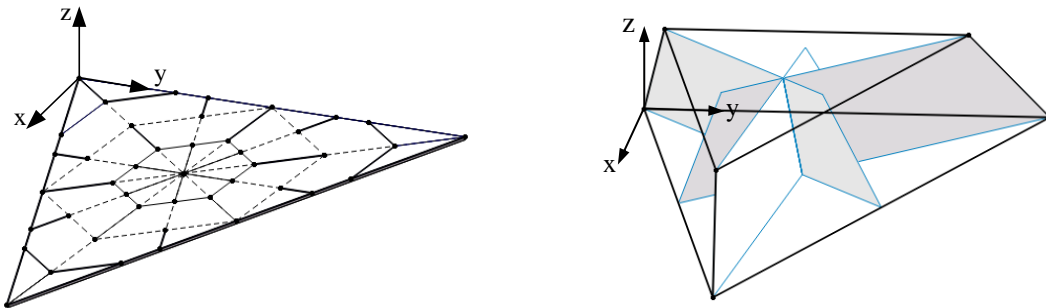
Table 2: Maximum linear dimensions of the three-way orthogonal pattern

Direction($i=x, y, z$)	x	y	z
i_{\max}^u	$\sqrt{3}l$	$2l$	s
i_{\max}^f	$\frac{3}{4}l$	$\frac{\sqrt{3}}{2}l$	$d = \frac{\sqrt{3}}{2n}l (n \leq 3)$ $\frac{1}{2\sqrt{3}}l (n > 3)$
r_i	$\frac{4}{\sqrt{3}}$	$\frac{4}{\sqrt{3}}$	$\frac{2ns}{\sqrt{3}l} (n \leq 3)$ $2\sqrt{3}\frac{s}{l} (n > 3)$

The table shows that the linear dimension ratios in direction x and y are constant and independent of n , and the largest linear dimension ratio in direction z is given by $2\sqrt{3}\frac{s}{l}$ when $n \geq 3$. As a result, when $n \geq 3$ the maximum linear dimensions of the folded configuration are invariant of n .

3.1.3 Triangle from hexagon.

As described in the paper model in Fig. 8, the equivalent models of the unfolded and folded configurations of the triangle from hexagon based on leaf-in pattern are illustrated in Fig. 12.



(a) Equivalent model of the unfolded state

(b) Equivalent model of the folded state

Fig. 12: Equivalent models of the unfolded and folded states of the triangle from hexagon based on leaf-in pattern

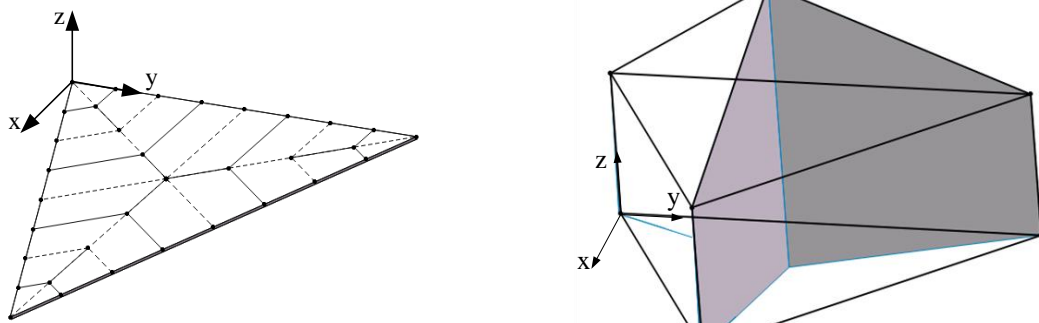
Table 3 reports the maximum linear dimensions and linear dimension ratios in the different directions. It can be observed that the linear dimension ratios in directions x and y are constant, while the linear dimension ratio in direction z, for a given ratio of $\frac{s}{l}$, is proportional to n, the quantity of radial creases in a triangle.

Table 3: Maximum linear dimensions of triangle from hexagon based on leaf-in pattern.

Direction($i=x, y, z$)	x	y	z
i_{\max}^u	$\frac{3}{2}l$	$\sqrt{3}l$	s
i_{\max}^f	$\frac{\sqrt{3}}{2}nd\left(\frac{3}{4}l\right)$	$nd\left(\frac{\sqrt{3}}{2}l\right)$	$d\left(\frac{\sqrt{3}}{2n}l\right)$
r_i	2	2	$\frac{2n}{\sqrt{3}} \cdot \frac{s}{l}$

3.1.4 Triangle based on leaf-out pattern.

Similarly, the equivalent models of the unfolded and folded configurations of the triangle based on leaf-out pattern are described in Fig. 13.



(a) Equivalent model of the unfolded state

(b) Equivalent model of the folded state

Fig. 13: Equivalent model of unfolded and folded state of triangle based on leaf-out pattern

The maximum linear dimensions of the triangle based on leaf-out pattern are obtained following the same procedure and the results summarized in Table 4 show that only the linear dimension ratio in direction z is constant for a given value of $\frac{S}{l}$, while the linear dimension ratios in direction x and y are identical and proportional to n , the quantity of radial creases in a triangle unit.

Table 4: Maximum linear dimensions of triangle based on leaf-out pattern

Direction ($i=x, y, z$)	x	y	z
l_{\max}^u	$\frac{3}{2}l$	$\sqrt{3}l$	s
l_{\max}^f	$\frac{3}{2}d$	$\sqrt{3}d$	$\frac{l}{2}$
r_i	$\frac{2n}{\sqrt{3}}$	$\frac{2n}{\sqrt{3}}$	$\frac{2s}{l}$

3.2 Deployment ratio

Due to the limitations imposed by transportation conditions, space membrane mechanisms need to be folded before launch and deployed in orbit. Therefore, the deployment ratio is a crucial design index (Deng 2013). The deployment ratio of the membrane folding mode is defined here as the ratio of the deployment volume to the folded volume, given by the formula: $\Theta = V_d/V_f$ where Θ is the deployment ratio, V_d is the deployment envelope volume, and V_f is the folded envelope volume. The detailed calculations are given in the Appendix, and only the final results are reported here. A larger value of Θ is desirable in order to package a given membrane in as small a volume as possible during transportation.

3.2.1 Triangle based on orthogonal pattern.

The deployment ratio of the triangle based on orthogonal pattern is obtained as

$$\Theta = \frac{n}{2n-1} \quad (6)$$

The deployment ratio curve of the triangle based on orthogonal pattern is plotted as a function of the number of radial creases n in Fig. 14. The graph shows that the deployment ratio Θ rapidly decreases with the increase of the number of radial creases in a triangle unit n , but that the initial trend slows with $n > 4$ tending towards a value of 0.5 for large n .

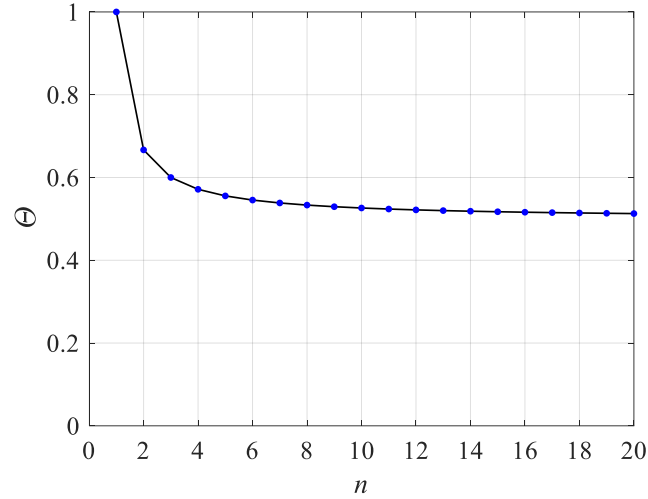


Fig. 14: Deployment ratio curve of the triangle based on orthogonal pattern with respect to crease parameters.

3.2.2 Three-way orthogonal pattern.

As for the triangle based on three-way orthogonal pattern, the deployment ratio Θ can be expressed as,

$$\Theta = \begin{cases} \frac{32n^3}{\sqrt{3}(3n^2 - 3n + 1)} \cdot \frac{s}{l} & n \leq 3 \\ \frac{32n^3}{\sqrt{3}(3n^2 - 3n + 1) + \frac{1}{\sqrt{3}}(n-3)^3} \cdot \frac{s}{l} & n > 3 \end{cases} \quad (7)$$

For a given value of s/l , Fig. 15 illustrates the deployment ratio curve of a triangular membrane based on three-way orthogonal pattern as a function of the number of creases n . The deployment ratio $\Theta(s/l)$ initially increases when n is less than 9 and then decreases with increasing n . The curve reaches its peak when the quantity of radial creases in a triangle unit n equals to 9.

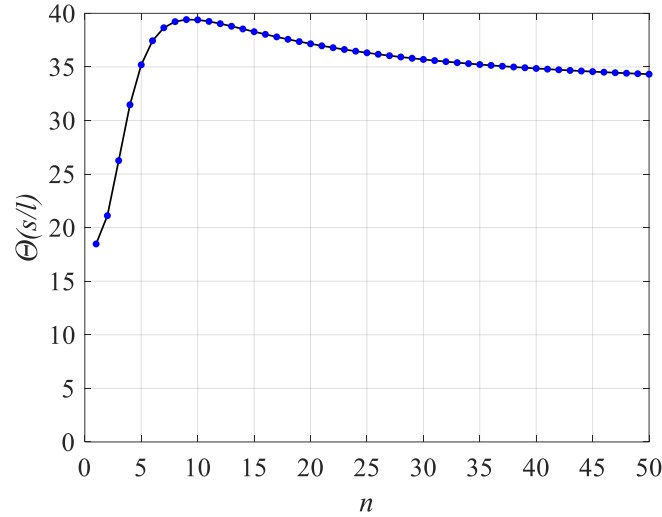


Fig. 15: Deployment ratio curve of three-way orthogonal pattern with respect to crease parameters

3.2.3 Triangle from hexagon.

The deployment ratio of the triangle from hexagon can be simplified as:

$$\Theta = \frac{24n^3}{3n^2 - 3n + 1} \cdot \frac{s}{l} \quad (8)$$

For a given ratio of s/l , the deployment ratio curve of the triangle from hexagon with respect to the number of creases n is plotted in Fig. 16 and shows $\Theta(s/l)$ increases with increasing n for all values of n .

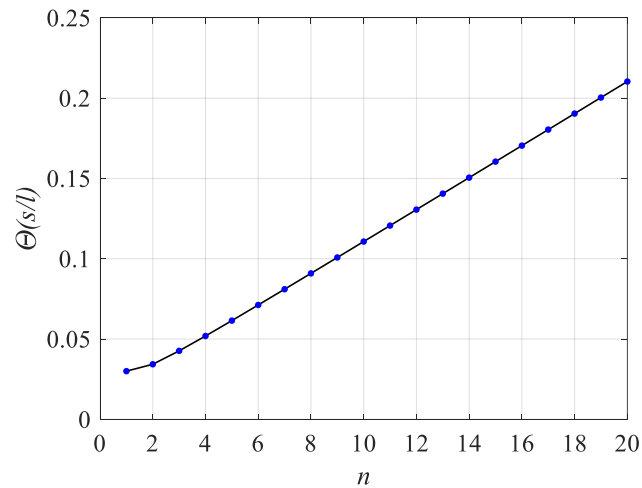


Fig. 16: Deployment ratio curve of triangle from hexagon with respect to crease parameters

3.2.4 Triangle based on leaf-out pattern.

The deployment ratio of the triangle based on leaf-out pattern is obtained as

$$\Theta = \frac{8n^3}{3n-2} \cdot \frac{s}{l} \quad (9)$$

With a given ratio of s/l , the deployment ratio curve of triangle from hexagon is plotted in Fig. 17 as a function of n . The deployment ratio $\Theta (s/l)$ increases with increasing n for all values of n .

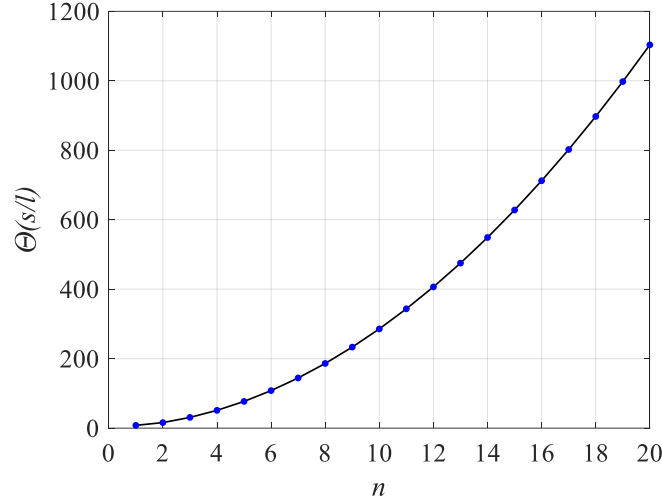


Fig. 17: Deployment ratio curve of triangle composed of half units with respect to crease parameters

3.3 Total length of creases

The creases have a direct impact on the overall level of accuracy of the folded structure; the total length of creases is a measure of the complexity of the initial folding arrangement, and a larger crease length increases the potential for damage in the membrane material. As the membrane explored in this paper is ultrathin and has practically zero bending stiffness, the deployable membrane can be regarded as wrinkle-free(Li, Zhu et al. 2021, Li, Li et al. 2022), making creases more influential in avoiding possible shape accuracy loss. Therefore, it is valuable to quantify the total crease length L such that this is kept to a manageable quantity in design. The following paragraphs investigate the performance of the alternatives presented in the Par.3.1 and Par.3.2 in terms of the total crease length L .

3.3.1 Triangle based on orthogonal pattern.

Creases of triangle based on orthogonal pattern are mainly divided into tangential and radial creases. The total

length of the radial creases is $\frac{\sqrt{3}l}{2}$, and tangential creases are equivalent to $n-1$ creases with a length of $\frac{l}{2}$, as

shown in its creases diagram. Therefore, the total length of creases is given as

$$L = \frac{\sqrt{3}}{2}l + \frac{n-1}{2}l = \frac{n+\sqrt{3}-1}{2}l \quad (10)$$

3.3.2 Three-way orthogonal pattern.

The three-way orthogonal pattern is made up of symmetrical triangle units with $\alpha = \frac{\pi}{2}$ and one additional triangle placed at the centre. Thus, its total length of creases is three times the total creases length of the triangle unit added to the length of the creases of the central triangle:

$$L = 3 \times \frac{n + \sqrt{3} - 1}{2} l + 3l + 3 \times \frac{\sqrt{3}}{2} l = \left(\frac{3}{2} n + 3\sqrt{3} + \frac{3}{2} \right) l \quad (11)$$

3.3.3 Triangle from hexagon.

As shown in Fig. 18, the creases of this new triangle are divided in two typologies: creases labelled in blue with fixed total length and six identical parts labelled in yellow. According to the symmetry and the geometry, the total length of constant creases L_1 labelled in blue is derived as,

$$L_1 = 3l + 3 \times \frac{l}{2} + 6 \times \frac{l}{\sqrt{3}} = \left(\frac{9}{2} + 2\sqrt{3} \right) l \quad (12)$$

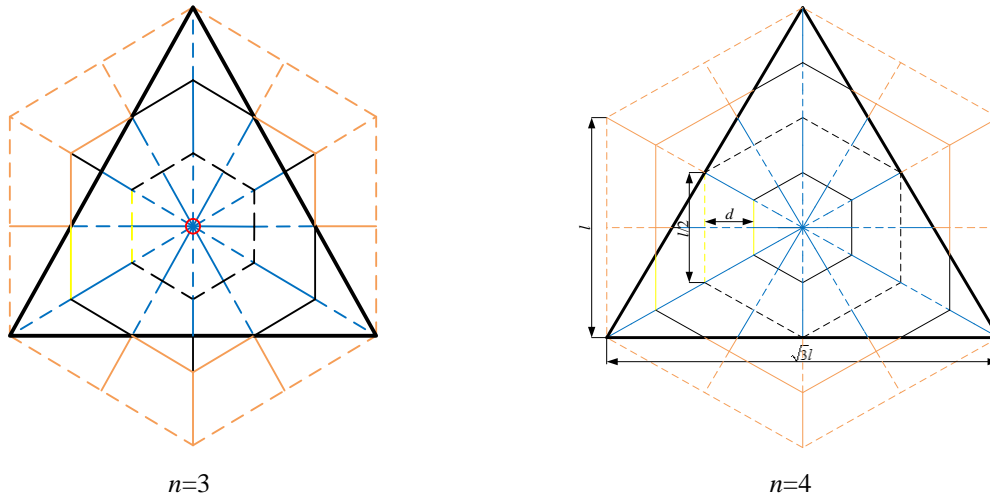


Fig. 18: Crease calculation of triangle from hexagon based on leaf-in pattern

The total length of the creases labelled in yellow L_2 is determined by the parity (odd-even) of the number of radial creases in a triangle unit n , and defined as

$$L_2 = \begin{cases} \left(1 + \frac{n-1}{2} \right) \times \frac{n-1}{2} \times \frac{l}{n} = \frac{n^2-1}{4n} l & n \text{ is odd} \\ \frac{1}{2} \left(\frac{2}{n} \times \frac{l}{2} + \frac{l}{2} \right) \times \frac{n}{2} \times 2 - \frac{l}{2} = \frac{n}{4} l & n \text{ is even} \end{cases} \quad (13)$$

Hence the total length of creases for the triangle from hexagon pattern is given as

$$L = L_1 + 6L_2 = \begin{cases} \left(\frac{3n^2 - 3}{2n} + \frac{9}{2} + 2\sqrt{3} \right) l & n \text{ is odd} \\ \left(\frac{3n}{2} + \frac{9}{2} + 2\sqrt{3} \right) l & n \text{ is even} \end{cases} \quad (14)$$

3.3.4 Triangle based on leaf-out pattern.

According to the geometry and the internal symmetry, the triangle based on leaf-out pattern can be divided into three identical parts, each one with a crease length equivalent to n creases with a length of $\frac{l}{2}$. Thus, the total length of creases is given by

$$L = 3l + 3 \times \frac{n}{2} l = \left(\frac{3}{2}n + 3 \right) l \quad (15)$$

3.4 Total number of junctions

For deployable membranes, the junctions where the creases meet are critical points where peak folding stresses will occur. Therefore, for membrane folding, it is valuable to count the number of multi-fold junctions. Additionally, the type of junction, whether it is a simple 4-fold junction or a higher order junction, is also of significance. This section explores how the number of radial creases in a triangle unit n determines the number and type of junctions in the different crease patterns. The case $n=4$ will be selected for the illustrations as it is the simplest case that involves all types of fold junctions.

3.4.1 Triangle based on orthogonal pattern.

As plotted in Fig. 19, there are three junctions in total, which are all junctions of four creases circled in black. Among them, there are two junctions of three crest and one valley, and one junction of three valley and one crest. In the general case, the total number of junctions can be summed up as $N=n-1$.

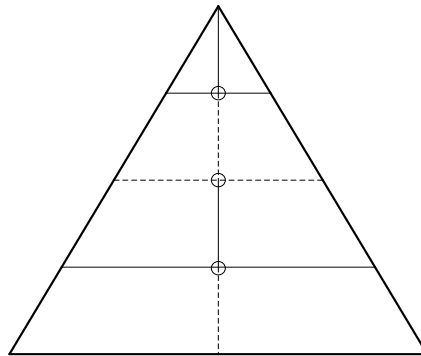


Fig. 19: Junctions (shown as circles) of the triangle based on orthogonal pattern for $n=4$.

3.4.2 Three-way orthogonal pattern.

Compared with the junctions of the triangle based on orthogonal pattern, the junctions of the three-way orthogonal pattern are more complex, even with $\alpha < 90^\circ$. In Fig. 20, when $n = 4$, there are three types of junctions, including junctions of four creases with $\alpha = 90^\circ$ labelled in black, junctions of three creases with $\alpha < 90^\circ$ labelled in purple, and a central junction of six creases labelled in green. In the general case, the total number of junctions for the triangle composed of triangle units can be represented as $N = 3n + 4$.

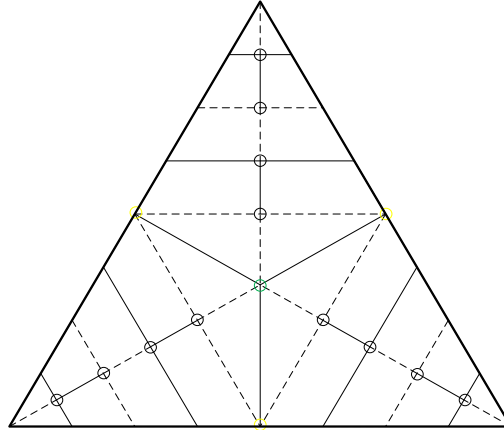


Fig. 20: Junctions of the triangle composed of triangle units for $n=4$.

3.4.3 Triangle from hexagon.

In the case of the triangle from hexagon pattern, the type and number of junctions are both related to the parity of n . The junctions are plotted and labelled in Fig. 21 for the cases $n=1,2,3$ and 4, and summarized in Table 5. It is possible to observe the emergence of edge junctions of three creases labelled in purple while n is even and the emergence of edge junctions of two creases labelled in orange. According to the parity of n , the total number of junctions for a triangle from hexagon is given as

$$N = \begin{cases} 4.5n - 3.5 + 6 \times [2n/3] & n \text{ is odd} \\ 7.5n - 2 & n \text{ is even} \end{cases} \quad (16)$$

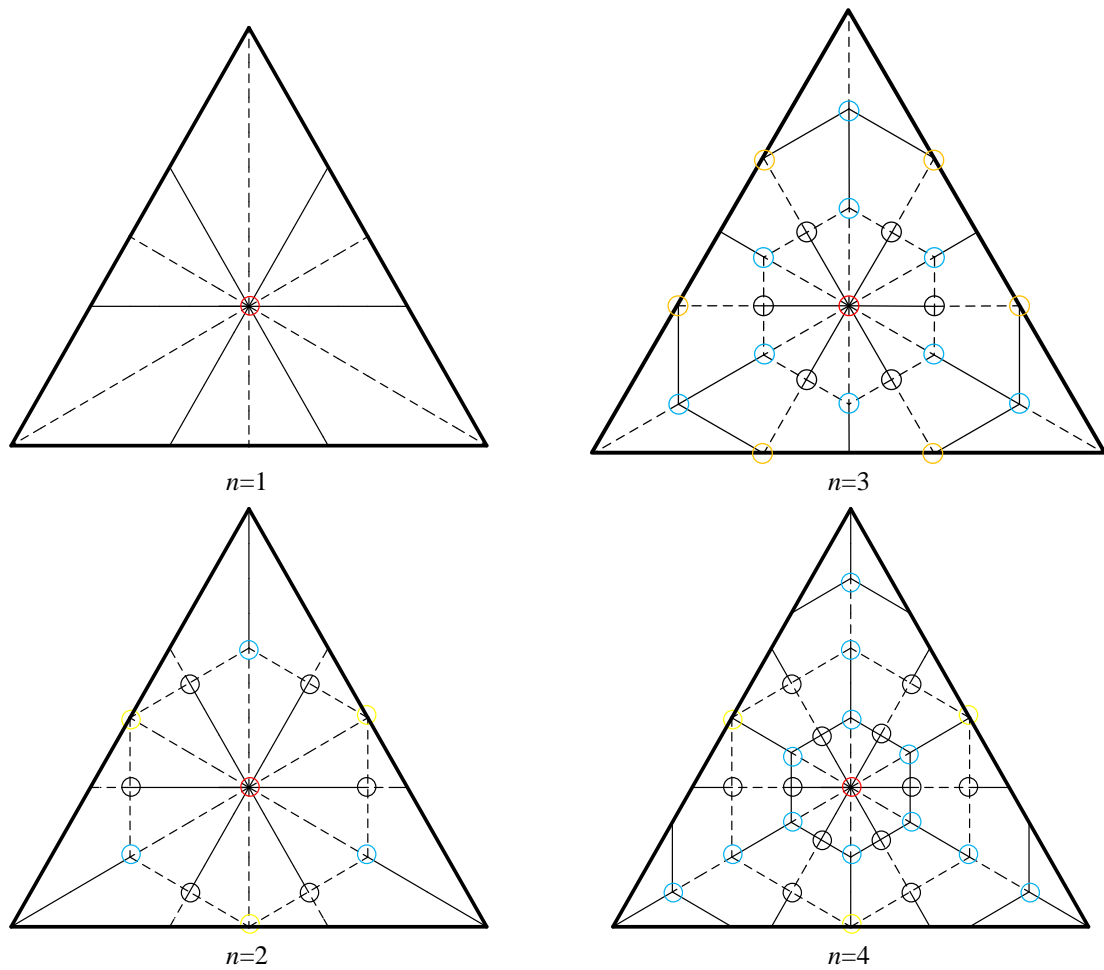


Fig. 21: Junctions of the triangle from hexagon for the cases $n=1$ to 4.

Table 5: Type and number of junctions of the triangle from hexagon

n	junctions of 4 creases		junctions of 3 creases (yellow)	junctions of 12 creases (red)	junctions of 2 creases (orange)	N
	$\alpha=90^\circ$ (black)	$\alpha < 90^\circ$ (blue)				
1	0	0	0	1	0	1
2	6	3	3	1	0	13
3	6	9	0	1	6	22
4	12	12	3	1	0	28

3.4.4 Triangle based on leaf-out pattern.

For the triangle based on leaf-out pattern, there are only two types of junctions: junctions of four creases with $\alpha < 90^\circ$ labelled in blue and junctions of six creases labelled in green. In the general case, the total number of junctions can be calculated as $N=3n-2$.

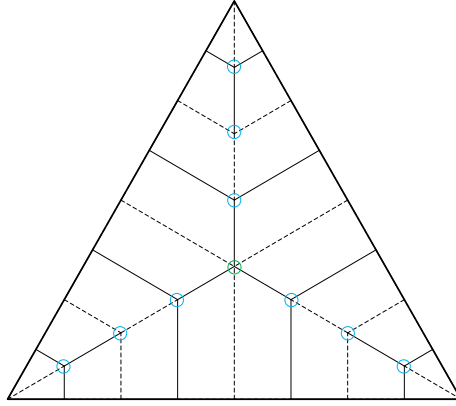


Fig. 22: Junctions of the triangle based on leaf-out pattern for $n=4$.

3.5 Deployment sequence

The deployment mode and the number of the deployment stages directly determine the deployment complexity of a membrane structure, and influence the deployment scheme of the triangular geometry that needs to be designed. The number of deployment sequence is a critical factor affecting the deployment efficiency and valuable measure of complexity. In order to facilitate the deployment from the folded configuration and achieve the flat triangular surface, only the three corners are allowed tension and the other vertices are free to move in all directions. Compared with the other three creases patterns, only the triangle based on orthogonal pattern requires two deployment sequence, because its three corners need to be tensioned in two perpendicular directions, corresponding to two stages. As for the other three creases patterns, their three corners only need to be extended simultaneously along the three central lines of the triangle to conduct the one-sequence deployment. The reason for this phenomenon is that only the triangle based on orthogonal pattern does not have crease dip angle $\alpha < 90^\circ$, while $\alpha=90^\circ$ corresponds to a two-sequence deployment, which decreases deployment efficiency.

4 Results and Discussions

This section offers a comparison of the biomimetic folding investigated in section 3 and provides data which can help designers to arrive at an informed decision in the selection of the ideal folding pattern for a given application. The evaluation indices of the four different biomimetic folding patterns are summarized in Table 6, including the total length of creases L , the deployment ratio Θ and the total number of junctions N . In the comparison of the total length of the creases, the effect of the different side length a has been addressed introducing the ratio $\eta_L = \frac{L}{a}$, where L is the total length of creases and a is the side length of the triangle.

Fig. 23 illustrates the relationship between the deployment ratio Θ , and the ratio of the total length of creases to the side length, η_L . The ordinate is the deployment ratio Θ while the abscissa η_L ranges from 0 to 50. Given that the unit for the vertical axis includes the factor s/l , the cases of [paper model](#) [$l=100\text{mm}$, $s = 125\mu\text{m}$] and [scaled deployable membrane prototype](#) [$l=1000\text{mm}$, $s = 125\mu\text{m}$] are shown. Fig. 23 shows that the value of Θ increases with increasing η_L for the three-way orthogonal pattern, triangle from hexagon and triangle based on leaf-out, while the Θ of the triangle based on orthogonal pattern decreases with increasing η_L , especially for small values of η_L . Moreover, when η_L is less than 10, the Θ value for the triangle based on orthogonal pattern is considerably higher than the corresponding value of the other crease patterns with the same η_L . However, Fig. 23 highlights an interesting aspect - the deployment ratio Θ of the triangle based on leaf-out pattern exceed that of the other alternatives, included triangle based on orthogonal pattern, when η_L is greater than 35.

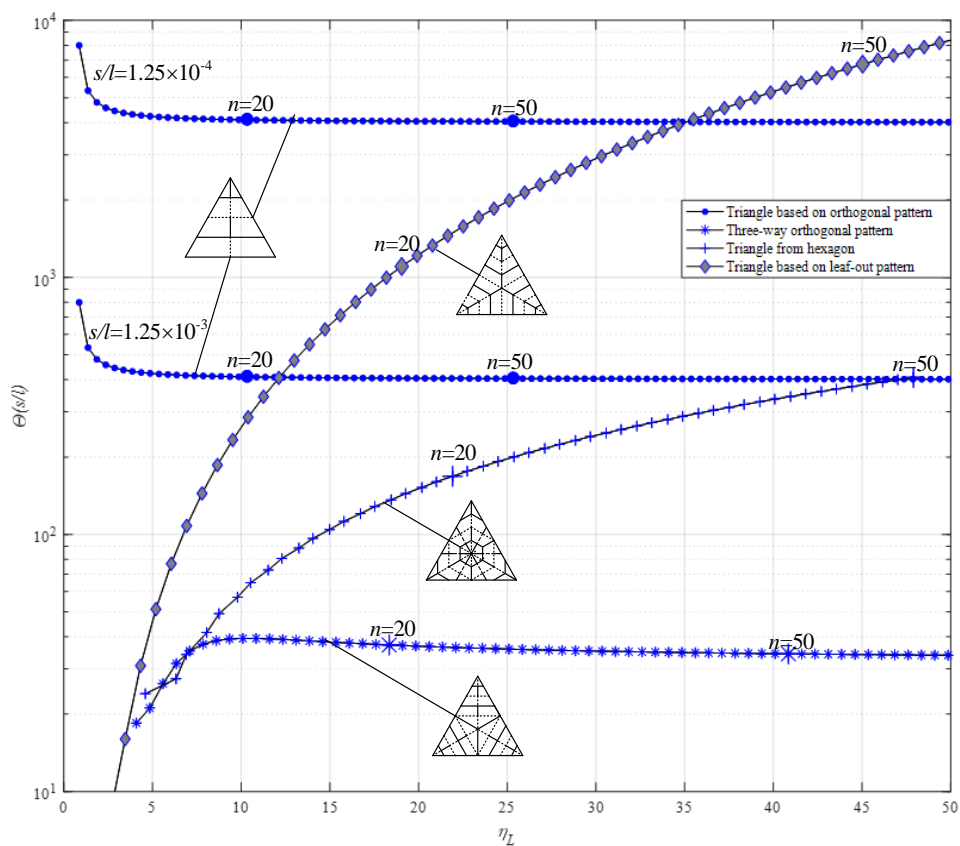
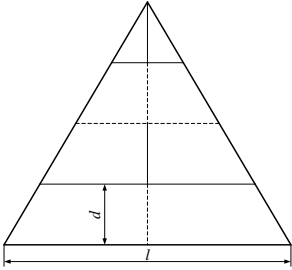
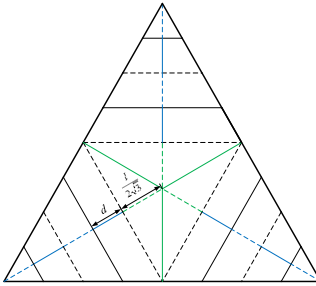
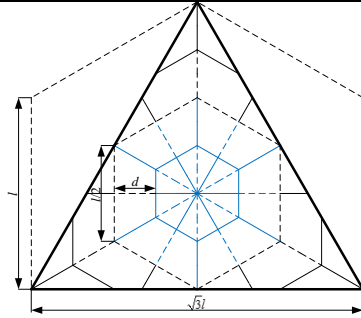
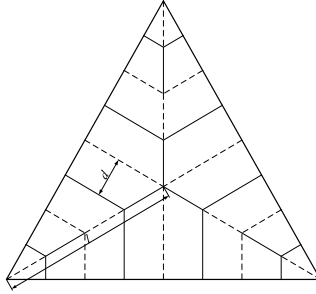


Fig. 23: Relations between the deployment ratio Θ and ratio of total length of creases to the side length η_L

Table 6: Comparison of different biomimetic folding pattern performance indices.

	Triangle based on orthogonal pattern	Three-way orthogonal pattern	Triangle from hexagon	Triangle based on leaf-out pattern
Creases diagram				
side length- <i>a</i>	l	$2l$	$\sqrt{3}l$	$\sqrt{3}l$
L	$\frac{n+\sqrt{3}-1}{2}l$	$\left(\frac{3}{2}n+3\sqrt{3}+\frac{3}{2}\right)l$	$\begin{cases} \left(\frac{3n^2-3}{2n}+\frac{9}{2}+2\sqrt{3}\right)l & n=2i-1 \\ \left(\frac{3n}{2}+\frac{9}{2}+2\sqrt{3}\right)l & n=2i \end{cases}$	$\left(\frac{3}{2}n+3\right)l$
$\eta_L = \frac{L}{a}$	$\frac{n+\sqrt{3}-1}{2}$	$\frac{3}{4}n+\frac{3}{2}\sqrt{3}+\frac{3}{4}$	$\begin{cases} \frac{\sqrt{3}n^2-\sqrt{3}}{2n}+\frac{3}{2}\sqrt{3}+2 & n=2i-1 \\ \frac{\sqrt{3}}{2}n+\frac{3}{2}\sqrt{3}+2 & n=2i \end{cases}$	$\frac{\sqrt{3}}{2}n+\sqrt{3}$
Θ	$\frac{n}{2n-1}$	$n \leq 3 \frac{32n^3}{\sqrt{3}(3n^2-3n+1)} \cdot \frac{s}{l}$ $n > 3 \frac{32n^3}{\sqrt{3}(3n^2-3n+1)+\frac{1}{\sqrt{3}}(n-3)^3} \cdot \frac{s}{l}$	$\frac{24n^3}{3n^2-3n+1} \cdot \frac{s}{l}$	$\frac{8n^3}{3n-2} \cdot \frac{s}{l}$
N	$n-1$	$3n+4$	$\begin{cases} 4.5n-3.5+6 \times [2n/3] & n=2i-1 \\ 7.5n-2 & n=2i \end{cases}$	$3n-2$

Similarly, the relationship between the deployment ratio Θ and the total number of junctions N is plotted in Fig. 24 for the range of patterns studied here. When N is over 70, the curve of the triangle from hexagon begins to show zig-zag fluctuations, as the calculation of N depends on the parity of n . Furthermore, the triangle based on leaf-out pattern has a higher value of Θ when N is greater than 110.

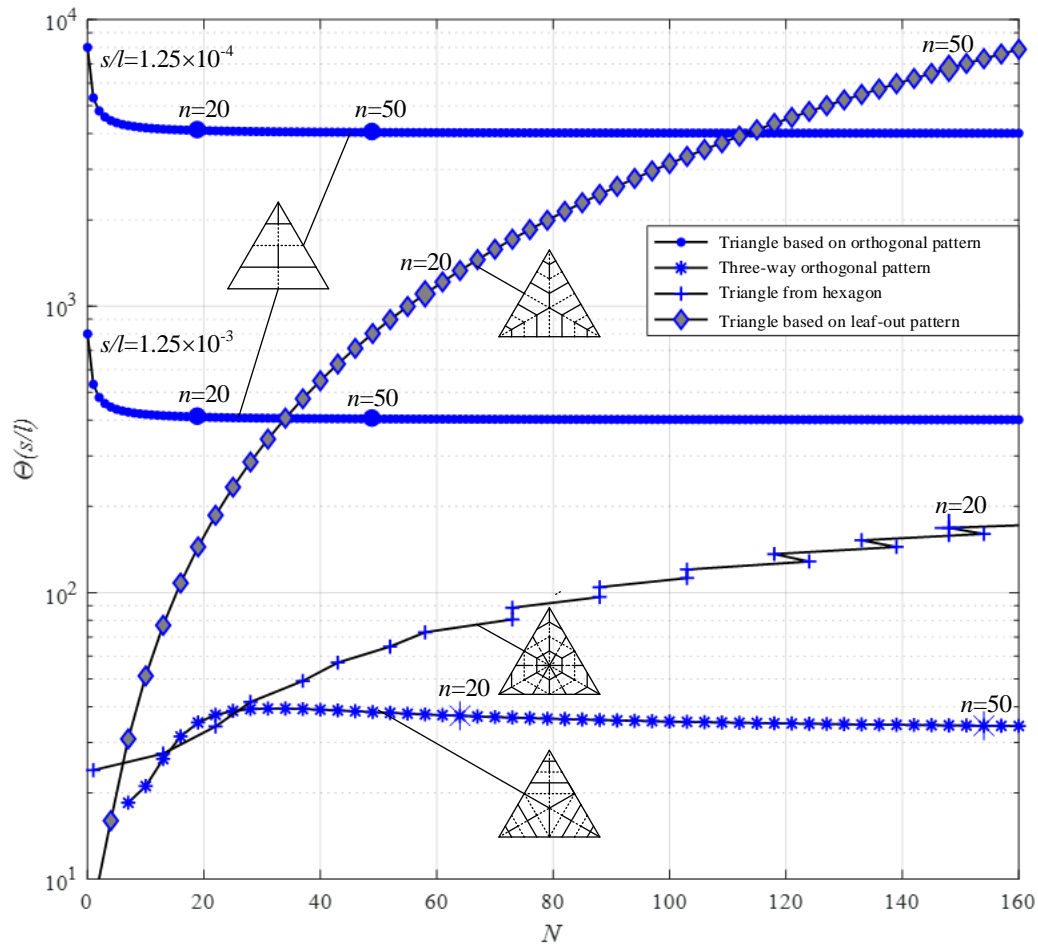


Fig. 24: Relations between the deployment ratio Θ and total number of junctions N

Fig. 25 shows the relationship between the ratio of the total length of creases to the side length η_L , and the total number of fold junctions N . The behaviour is approximately linear for all crease patterns, but zigzag fluctuations of the curve for the triangle from hexagon pattern can be observed. The lower the value of the ratio of total length of creases to the side length η_L , the easier the manufacturing of the folded membrane. In view of this, the triangle based on orthogonal pattern has the largest value of η_L for a given value of N compared with the other three creases patterns.

For the given application with stringent surface accuracy requirements, such as membrane antenna and optical spacecraft in high-resolution observation and communication space missions, the ratio of the total length of creases to the side length η_L and the total number of fold junctions N act more principal indicator of the selection

folding pattern than the deployment ratio Θ . Therefore, on the premise of meeting the requirements of deployment ratio, the triangle from hexagon pattern has a better crease design for the given application because of the lowest value of η_L for a given value of N compared with the other three creases patterns as illustrated in Fig. 25, high geometrical symmetry and deployment efficiency. Nevertheless the solar sail requires high deployment ratio but not shape accuracy, the triangle based on leaf-out pattern can obtain larger deployment ratio by reasonable design of the number of radial creases n under comprehensive consideration of other evaluation indices, resulting in it being chosen as the most appropriate folding pattern.

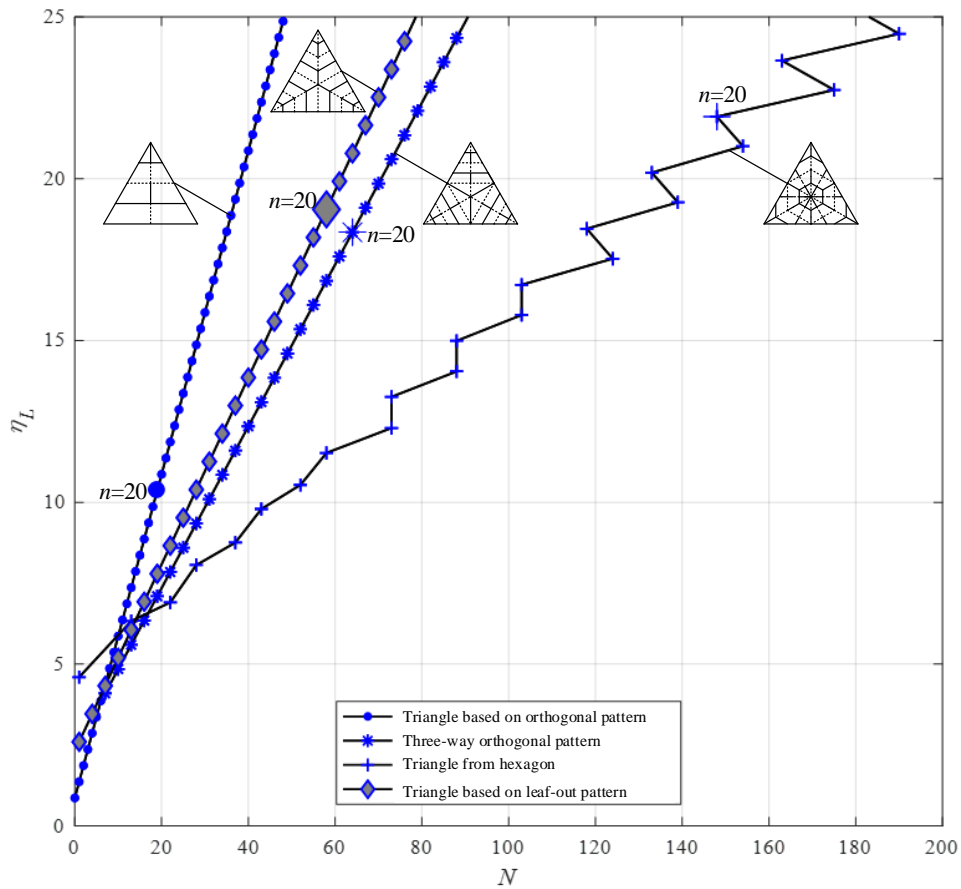


Fig. 25: Relations between the ratio of total length of creases to the side length η_L and total number of junctions N

5 Conclusions

The study of biomimetic folding and origami methods, to design and evaluate the creases patterns of space deployable membranes, is in current trends. This paper introduces the geometric design of the basic unit of biomimetic folding, including leaf-in pattern, leaf-out pattern and orthogonal pattern distinguished by the vein angle, and applies the basic units to design the creases patterns of triangular membrane. The feasibility and folded configuration of various biomimetic folding patterns are then investigated with paper models. And evaluation

indices considering linear dimension, three-dimensional space, deployment efficiency and prototype manufacturing for folding method of membrane are established and applied in the assessment of the following promising folding pattern alternatives: triangle based on orthogonal pattern, three-way orthogonal pattern, triangle from hexagon and triangle based on leaf-out pattern. Based on the evaluation indices, a parametric study is summarized in charts and tables with data which aims to support an informed decision in the selection of the ideal biomimetic folding pattern and to reveal the relationship between geometric parameters and crease pattern performance indices. The work presented in this paper, to the author's knowledge, is the first implementation of evaluation indices to develop triangular deployable membranes based on biomimetic folding.

This study endorses the exploitation of basic unit and creases patterns of biomimetic folding to produce deployable triangles. On the other hand, the geometric design process and evaluation indices analysis presented in this paper pave the way to design more novel creases patterns with exhilarating features and conduct more comprehensive evaluation for deployable space membrane structures.

Acknowledgements

This work was supported by the National Natural Science Foundations of China (Grant Nos. 51835002) and the Programme of Introducing Talents of Discipline to Universities ("111 Programme"). The support provided by China Scholarship Council (CSC) during a visit of Yuzhen Tang to University of Nottingham is acknowledged.

Appendix

Appendix A Detailed calculations of deployment ratio

A.1 Triangle based on orthogonal pattern.

Starting from the geometric relationship and creases diagram of the triangle based on orthogonal pattern, it is possible to obtain the deployment volume and folded volume. The deployment volume is equivalent to the volume of the corresponding triangular prism with the height equivalent to the membrane thickness and it is expressed as:

$$V_d = \frac{\sqrt{3}}{4} l^2 s \quad (A1)$$

As shown in Fig. 10, the folded state of the triangle based on orthogonal pattern is equivalent to a prism with the base coincident with the parallelogram highlighted in grey in Fig. 7(a) and the height equal to $2ns$. As a result, the folded volume is derived as:

$$V_f = \frac{1}{2} \left(\frac{n-1}{2n} l + \frac{1}{2} l \right) d \cdot 2ns = \frac{2n-1}{2} dls \quad (\text{A2})$$

Substituting Eq.(4) to Eq.(A2), the folded volume of triangle membrane is given by the formula,

$$V_f = \frac{\sqrt{3}(2n-1)}{4n} l^2 s \quad (\text{A3})$$

According to the definition of deployment ratio, the deployment ratio of the triangle based on orthogonal pattern is expressed as,

$$\Theta = \frac{n}{2n-1} \quad (\text{A4})$$

A.2 Three-way orthogonal pattern.

Similarly, also for the three-way orthogonal pattern, the deployment volume can be obtained from the corresponding triangular prism with the height equivalent to the membrane thickness. In this case the side length equals to $2l$ and, as a result, the deployment volume is derived as:

$$V_d = \sqrt{3} l^2 s \quad (\text{A5})$$

Fig. 11 illustrates the correlation between the folded volume and then number of creases n . When $n \leq 3$, the folded volume is equivalent to a triangular frustum of a pyramid, with the assumption that the thickness of the membrane is negligible. According to this geometric similarity, when $n \leq 3$ the folded volume is given by:

$$V_f = \frac{(3n^2 - 3n + 1)\sqrt{3}}{12} d^3 \quad (n \leq 3) \quad (\text{A6})$$

When $n > 3$, the folded configuration is described by a triangular frustum of a pyramid combined with a triangular pyramid. The volume of the triangular pyramid V_t is expressed by:

$$V_t = \frac{3\sqrt{3}}{4} \left(\frac{l}{2\sqrt{3}} - d \right)^3 \quad (\text{A7})$$

As a result, the total folded volume with $n > 3$ is given by:

$$V_f = \frac{(3n^2 - 3n + 1)\sqrt{3}}{12} d^3 + \frac{3\sqrt{3}}{4} \left(\frac{l}{2\sqrt{3}} - d \right)^3 \quad (n > 3) \quad (\text{A8})$$

Substituting Eq.(A5), (A6) and (A8) to the definition of deployment ratio, the following equation is derived as

$$\Theta = \begin{cases} \frac{12l^2s}{(3n^2 - 3n + 1)d^3} & n \leq 3 \\ \frac{12l^2s}{(3n^2 - 3n + 1)d^3 + 9\left(\frac{l}{2\sqrt{3}} - d\right)^3} & n > 3 \end{cases} \quad (\text{A9})$$

According to the numerical relationship between the crease parameters mentioned above, Eq.(A9) can be rewritten as,

$$\Theta = \begin{cases} \frac{32n^3}{\sqrt{3}(3n^2 - 3n + 1)} \cdot \frac{s}{l} & n \leq 3 \\ \frac{32n^3}{\sqrt{3}(3n^2 - 3n + 1) + \frac{1}{\sqrt{3}}(n-3)^3} \cdot \frac{s}{l} & n > 3 \end{cases} \quad (\text{A10})$$

A.3 Triangle from hexagon.

The folded configuration of the triangle from hexagon based on leaf-in pattern is a triangular prism with the height of membrane thickness and the side length of $\sqrt{3}l$. The deployment volume is derived as:

$$V_d = \frac{3\sqrt{3}}{4} l^2 s \quad (\text{A11})$$

The folded volume, based on a folded configuration equivalent to a triangular frustum of a pyramid and the assumption of a negligible thickness, can be expressed as:

$$V_f = \frac{(3n^2 - 3n + 1)\sqrt{3}}{12} d^3 \quad (\text{A12})$$

Therefore, its deployment ratio is calculated as:

$$\Theta = \frac{9l^2s}{(3n^2 - 3n + 1)d^3} \quad (\text{A13})$$

Since $d = \frac{\sqrt{3}l}{2n}$, Eq.(A13) can be simplified as:

$$\Theta = \frac{24n^3}{3n^2 - 3n + 1} \cdot \frac{s}{l} \quad (\text{A14})$$

A.4 Triangle based on leaf-out pattern.

The deployment volume of the triangular membrane based on leaf-out pattern is similar to the previous case described in par. A.3 and equals to $\frac{3\sqrt{3}}{4}l^2s$. As shown in Fig. 13, the folded configuration can be considered equivalent to a triangular prism combined with a triangular pyramid. With the assumption that the thickness of the membrane is negligible like in previous cases, the folded volume V_f can be calculated as:

$$V_f = \frac{3n-2}{4}d^3 \quad (\text{A15})$$

where $d = \frac{\sqrt{3}l}{2n}$ and Eq.(A15) can be rearranged as follows:

$$V_f = \frac{3\sqrt{3}(3n-2)}{32n^3}l^3 \quad (\text{A16})$$

According to the definition of deployment ratio, the deployment ratio of the triangle based on leaf-out pattern is obtained as,

$$\Theta = \frac{8n^3}{3n-2} \cdot \frac{s}{l} \quad (\text{A17})$$

Appendix B Creases parameters multi-objective optimization

Based on the evaluation indices established in section 3, creases parameters multi-objective optimization for the biomimetic folding patterns proposed above is conducted. Combined with the above research results, these evaluation indices are all taken as objective functions with the same level of priority, including deployment ratio Θ , the ratio of the total length of creases to the side length η_L and the total number of junctions N , as derived in follows.

$$\begin{cases} \text{Max} : \Theta \\ \text{Min} : \eta_L \\ \text{Min} : N \\ \text{integer } n \in [2, 50] \end{cases} \quad (\text{B1})$$

As for the settlements of the genetic algorithm, the uniform crossover and random selection type are adopted with the population size of 400 and the crossover rate of 0.9. When the variation rate is adjusted to 0.5, the multi-

objective optimization design parameters and results are obtained in Table B. Here the feasibility of optimization is discussed through the case in which equal requirements are given to both deployment ratio and shape accuracy, but for a given application such as the membrane antenna or solar sail expounded in Section 4, these objectives should be given different weights according to the special performance requirements in specific space missions, which warrant further study in subsequent research.

Table B1: Multi-objective optimization results for different biomimetic folding patterns

	Triangle based on orthogonal pattern	Three-way orthogonal pattern	Triangle from hexagon	Triangle based on leaf-out pattern
n	2	2	2	50
Θ	$2/3$	$\frac{256}{7\sqrt{3}} \cdot \frac{s}{l}$	$\frac{192}{7} \cdot \frac{s}{l}$	$\frac{250000}{37} \cdot \frac{s}{l}$
η_L	$\frac{\sqrt{3}+1}{2}$	$\frac{9}{4} + \frac{3}{2}\sqrt{3}$	$\frac{5}{2}\sqrt{3} + 2$	$26\sqrt{3}$
N	1	8	13	148

References

- Alhorn Dean, C. J., E. Agasid, C. Adams, G. Laue, C. Kitts and S. O'Brien (2011). Nanosail-d: The small satellite that could! 25th Annual AIAA/USU Conference on Small Satellites, Logan, UT, USA.
- Bao, H., S. White, B. Spence and S. Kiefer (2016). Commercialization of Deployable Space Systems' roll-out solar array (ROSA) technology for Space Systems Loral (SSL) solar arrays. 2016 IEEE Aerospace Conference, Big Sky, MT, USA.
- Chodimella, S., J. Moore, J. Otto and H. Fang (2006). Design Evaluation of a Large Aperture Deployable Antenna. 47th AIAA/ASME/ASCE/AHS/ASC Structures, Structural Dynamics, and Materials Conference 14th AIAA/ASME/AHS Adaptive Structures Conference 7th, Newport, Rhode Island.
- Deng, Z. (2013). Design of Space Deployable and Foldable Mechanisms, Harbin Institute of Technology Press.
- Focatiis, D. S. A. D. and S. D. Guest (2002). "Deployable membranes designed from folding tree leaves." Philosophical Transactions of the Royal Society of London. Series A: Mathematical, Physical and Engineering Sciences **360**(1791): 227-238.
- Furuya, H., Y. Inoue and T. Masuoka (2005). Deployment Characteristics of Rotationally Skew Fold Membrane for Spinning Solar Sail. 46th AIAA/ASME/ASCE/AHS/ASC Structures, Structural Dynamics and Materials Conference, Austin, Texas.
- Guest, S. D., and Pellegrino, S. (1992). Inextensional Wrapping of Flat Membranes. Proceedings of the First International Seminar on Structural Morphology, Montpellier.
- H.S.Patil and SiddharthVaijapurkar (2007). "Study of the Geometry and Folding Pattern of Leaves of Mimosa pudica." Journal of Bionics Engineering **04**(01): 22-26.
- Jianguo Cai, A. M. A., Xiaowei Deng, Yixiang Xu, and Jian Feng (2015). "Geometry and Motion Analysis of Origami-Based Deployable Shelter Structures." Journal of Structural Engineering **141**(10): 06015001.

Kobayashi, H., M. Daimaruya and H. Fujita (2003). Unfolding of Morning Glory Flower as a Deployable Structure. IUTAM Symposium on Dynamics of Advanced Materials and Smart Structures, Dordrecht.

Kobayashi, H., M. Daimaruya and J. Vincent (2000). Folding/Unfolding Manner of Tree Leaves as a Deployable Structure. Iutam-Iass Symposium on Deployable Structures: Theory and Applications, Springer: 211-220.

Kobayashi, H., B. Kresling and J. Vincent (1998). "The geometry of unfolding tree leaves." Proceedings of the Royal Society B Biological Sciences **265**(1391): 147-154.

Koryo, M. (1985). "Method of packaging and deployment of large membranes in space." The Institute of Space and Astronautical Science report **618**: 1-9.

Leipold, M., C. Widani, P. Groepper, C. Sickinger and F. Lura (2006). The european solar sail deployment demonstration mission. 57th International Astronautical Congress, Valencia, Spain.

Les Johnson , M., AndyHeaton, RobinPinson, GregLaue, CharlesAdams (2011). "NanoSail-D: A solar sail demonstration mission." Acta Astronautica **68**(5-6): 571–575.

Li, M., Y. Li, C. Zhang, G. Qi, Y. Sui, Y. Luo and J. Liu (2022). "Stiffness modulation-driven wrinkle-free membrane." Applications in Engineering Science **9**: 100087.

Li, M., K. Zhu, G. Qi, Z. Kang and Y. Luo (2021). "Wrinkled and wrinkle-free membranes." International Journal of Engineering Science **167**: 103526.

Mankins, J., N. Kaya and M. Vasile (2012). SPS-ALPHA: The First Practical Solar Power Satellite via Arbitrarily Large Phased Array (A 2011-2012 NIAC Project). 10th International Energy Conversion Engineering Conference, Atlanta, Georgia.

Mankins, J. C. (2002). "A technical overview of the "Suntower" solar power satellite concept." Acta Astronautica **50**(6): 369-377.

Mori Osamu, T. Y., Sawada Hirotaka and others (2010). "World's first mission of solar power sail by IKAROS." Space, Aeronautical and Navigational Electronics **110**(250): 155-160.

Nicholas Turner, B. G. a. M. S. (2016). "A review of origami applications in mechanical engineering." Proc IMechE Part C: J Mechanical Engineering Science **230**(14): 2345–2362.

Peraza Hernandez, E. A., Hartl, Darren J., Lagoudas, Dimitris C (2018). Active Origami: modeling, design, and applications, Springer.

Sasaki, S., K. Tanaka, K. Higuchi, N. Okuizumi, S. Kawasaki, N. Shinohara, K. Senda and K. Ishimura (2007). "A new concept of solar power satellite: Tethered-SPS." Acta Astronautica **60**(3): 153-165.

Talley, C., W. Clayton, P. Gierow, G. Laue and J. Moore (2006). Advanced Membrane Materials for Improved Solar Sail Capabilities. 43rd AIAA/ASME/ASCE/AHS/ASC Structures, Structural Dynamics, and Materials Conference: 3rd AIAA Gossamer Spacecraft Forum, Denver, Colorado.

Trautt, T. and S. White (2013). ST8 Ultraflex-175 Solar Array-Deployed Dynamics Analytical Modeling and Comparison to Validation Criteria. Aiaa Aerospace Sciences Meeting Including the New Horizons Forum & Aerospace Exposition, Orlando, Florida.

- Y. Chen, R. P., Z. You, (2015). "Origami of thick panels." Science **349** (6246): 396–400.
- Yang, Y., Y. Zhang, B. Duan, D. Wang and X. Li (2016). "A novel design project for space solar power station (SSPS-OMEGA)." Acta Astronautica **121**(2016): 51-58.
- Yuan, T. (2020). "Dynamic modeling for foldable origami space membrane structure with contact-impact during deployment." Multibody System Dynamics **50**(1): 1–24.
- Zhiqian Liu, H. Q., Xiao Li, et al. (2017). "Review of Large Spacecraft Deployable Membrane Antenna Structures." Chin. J. Mech. Eng **30**(6): 1447–1459.
- Zicai Shen, F. Z., Chunqing Zhao, Yuming Liu (2012). "Key Technology Analysis and Enlightenment of IKAROS Solar Sail." Spacecraft Engineering **21**(2): 101-107.
- Zirbel, S., B. Trease, M. Thomson, R. Lang, S. Magleby and L. Howell (2015). HanaFlex: a large solar array for space applications. Micro- and Nanotechnology Sensors, Systems, and Applications VII, Baltimore, Maryland, United States.
- Zirbel, S. A., R. J. Lang, M. W. Thomson, D. A. Sigel, P. E. Walkemeyer, B. P. Trease, S. P. Magleby and L. L. Howell (2013). "Accommodating Thickness in Origami-Based Deployable Arrays." Journal of Mechanical Design **135**(11): 111005.

Yuzhen Tang

E-mail: tangyuzhen@hit.edu.cn